Article

Light-Induced Length Shrinkage of Rod Photoreceptor Outer Segments

Yiming Lu[1], Jacopo Benedetti[1], and Xincheng Yao[1,2]

[1] Department of Bioengineering, University of Illinois at Chicago, Chicago, IL, USA
[2] Department of Ophthalmology and Visual Sciences, University of Illinois at Chicago, Chicago, IL, USA

Correspondence: Xincheng Yao, Bioengineering and Ophthalmology, University of Illinois at Chicago, Clinical Sciences North, Suite W103, Room 164D, 820 South Wood Street, Chicago, IL 60612, USA. e-mail: xcy@uic.edu

Purpose: This study was designed to verify light-induced outer segment (OS) length shrinkage of rod photoreceptors and to characterize its anatomic source at disc-level resolution.

Methods: Frog (*Rana pipiens*) retinas were used for this study. Time-lapse light microscopy of freshly isolated OSs was employed to test transient rod OS changes at 10 ms temporal resolution. Histological light microscopy of dark- and light-adapted retinas was used to confirm light-induced rod OS length changes; and transmission electron microscopy (TEM) was used to quantify light-driven structural perturbation of rod OSs at disc level resolution.

Results: Time-lapse light microscopy images verified transient length shrinking responses in freshly isolated rod OSs. Histological light microscopy images confirmed reduced rod OS lengths in light-adapted retinas, compared to that of dark-adapted retinas. TEM images disclosed shortened inter-disc distances in light-adapted retinas compared to dark-adapted retinas.

Conclusions: Light-induced rod OS length shrinkage was confirmed using time-lapse light microscopy of isolated rod OSs and histological light microscopy of dark- and light-adapted retinas. TEM revealed that the rod OS length shrinkage was correlated to the light-driven decrease of the space between individual discs, not the disc thickness itself.

Translational Relevance: Light-induced transient rod response promises a noninvasive biomarker for early diagnosis of age-related macular degeneration and retinitis pigmentosa, in which the rod photoreceptors are known to be more vulnerable than cone photoreceptors.

Introduction

Retinal photoreceptors are the cells in which phototransduction converts the light to electrophysiological signals. The process of phototransduction involves multiple cascaded chemical reactions that take place either on the discs or within their compartments in the outer segments (OSs) of the photoreceptors, including the sequential activation of rhodopsin/conopsin, G-protein and phosphodiesterase (PDE), and the hydrolysis of cyclic guanosine monophosphate (cGMP). The decrease in the intracellular cGMP concentration then results in hyperpolarization of the retinal photoreceptors.[1–3] Meanwhile, such chemical reactions are accompanied by structural perturbations that may produce stimulus-evoked intrinsic optical signal (IOS) changes in animal[4–8] and human retinas.[9] It is known that rod photoreceptors are more vulnerable than cone photoreceptors in age-related macular degeneration (AMD)[10,11] and retinitis pigmentosa (RP).[12] Recently, light-induced rod OS shrinkage and orientation movement have been observed in frog and mouse retinas.[13,14] OCT study has also revealed OS shrinkage in human retinas during light adapatation.[15] Comparative microscopy study has indicated that the light-induced OS change can be a primary contributor to the stimulus-evoked IOS,[16] and functional IOS distortions have been detected in animal retinas with retinal degeneration[17] and laser-produced dysfunc-
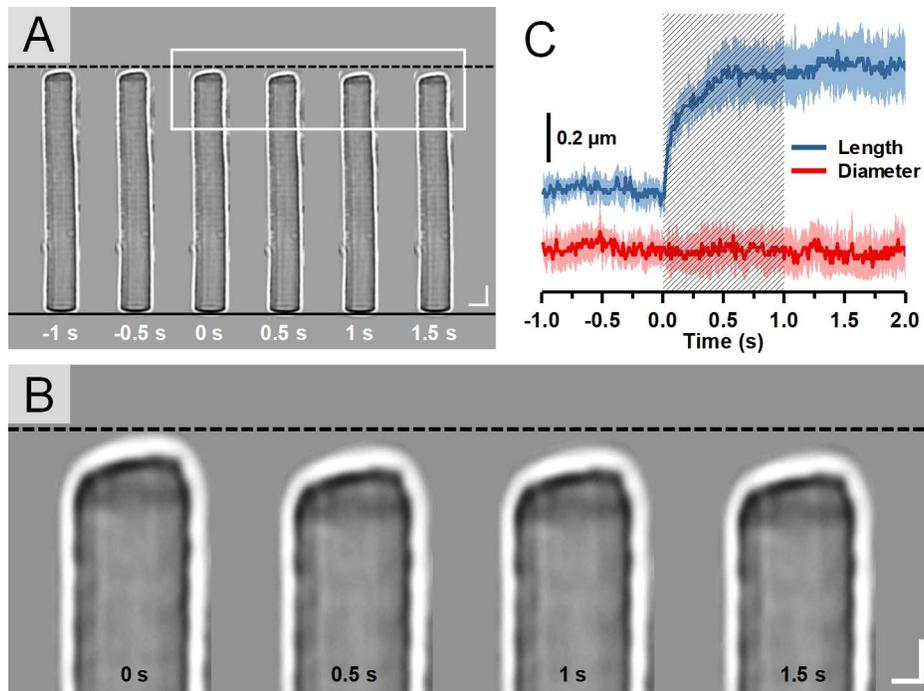
Figure 1. (A) Representative light microscopic images of a single isolated rod OS acquired with an interval of 0.5 seconds. To better show the light-evoked OS shrinkage, the base of the rod OS in each image is aligned horizontally as shown by the *black solid line* at the bottom. The *black-dashed line* at the top represents the position of the rod OS tip at time −1 second. *Scale bars* (in *white*) represent 5 μm. (B) Enlarged picture of the *white rectangle* in A. *Scale bars* (in *white*) represent 2 μm. (C) Time course of the averaged rod OS shrinkage in both length and diameter acquired from eight different rod OSs. *Colored areas* accompanying the curves represent the standard deviations. *Shaded area* indicates the 1-second stimulation period.

tion.[18] Therefore, a better understanding of rod OS responses offers the opportunity for functional imaging of rod physiology to assist with early diagnosis of retinal diseases. Comparative electrophysiological studies of freshly isolated retinas further revealed that such rod OS changes happen before hyperpolarization of the photoreceptors, indicating a disc-based physiological origin.[19] However, whether the physical origin of OS shrinkage is due to OS discs or interdisc space changes is still unknown.

This study was designed to investigate the light-induced conformational changes of rod OSs at a disc level. Frog (*Rana pipiens*) retinas were selected for this study as the frog rod photoreceptors are relatively large in diameter (∼5–8 μm)[20] compared to mouse rod photoreceptors (∼1–3 μm in diameter),[21] allowing unambiguous observations of OSs and relatively precise measurement of the changes in size. Multiple imaging modalities were applied in this study to explore the light-induced shrinkage of rod OSs. Time-lapse light microscopy was first employed to demonstrate the dynamic changes of freshly isolated rod OSs evoked by a visible light stimulus. Comparative histological imaging of dark- and light-adapted retinas were used to confirm the light-induced OS shrinkage. Transmission electron microscopy (TEM) of dark- and light-adapted retinas was employed to investigate the rod OS changes at disc resolution.

Methods

Sample Preparation

Retinal samples from leopard frogs (*R. pipiens*) were used for this study. For time-lapse microscopic imaging, eight isolated rod OSs were obtained from the isolated retinas of four dark-adapted frogs (Figs. 1A, 1B). Isolation of the retina was carried out following the protocol that has been reported in our previous publications.[16,19] Individual rod OSs were dissociated from the retina by finely chopping the retina with a razor blade and gently shaking the suspension solution containing the retinal cells and tissues.[22,23] The entire sample preparation was performed in oxygenated Ringer's solution containing 110.0 mM NaCl, 2.5 mM KCl, 1.6 mM MgCl$_2$, 1.0 mM CaCl$_2$, 22.0 mM NaHCO$_3$, 10.0 mM D-glucose with pH 7.3∼7.4 at room temperature (∼20°C). The

isolated rod OSs were then transferred to a chamber filled with Ringer's solution for dynamic light microscopic imaging.

For histological imaging analysis, two groups of complete retina-RPE-choroid-sclera complexes, that is, eyecups, were obtained from seven dark-adapted and seven light-adapted frogs (one eyecup from each frog), respectively. The eyecups were then immediately immersed in a fixative solution containing 4% para-formaldehyde (p-FA) and 1% glutaraldehyde (GA) buffered with 0.1 M sodium phosphate, pH 7.3.[24] All eyecups were fixated for at least 48 hours before cryosectioning. For the dark-adapted group, all the procedures were performed in a dark room under dim red light. After fixation, each eyecup was transferred from fixative to 300 μL 2.3 M sucrose buffered with 0.1 M sodium phosphate (pH 7.3 at 4°C) for 1 hour and was then embedded and quickly frozen in an optimal cutting temperature compound (Tissue-Tek; Sakura Finetek, Torrance, CA) to facilitate the cutting procedure. After cutting, the retinal samples were thawed, washed, and stained for light microscopic imaging.[25]

Another set of cryo-sectioned retinal samples, containing five dark-adapted and five light-adapted retinal samples from 10 different frogs, were further processed for TEM study. The thawing and washing process had been demonstrated to have negligible effect upon photoreceptor ultrastructure, and the acquired images were comparable in quality and the measurements were consistent with other published results.[24,26–29] After being thawed and washed, the retinal samples underwent a secondary fixation (osmication) as the lipid-rich structures (including membranes) were not well preserved by aldehydes.[30] This secondary fixation was performed using osmium tetraoxide (OsO_4), which also helped to stabilize proteins. Samples were then dehydrated through a graded series of ethanol (30%, 50%, 70%, 90%, 95%, and 100%) and were cut with an ultramicrotome diamond knife (Leica Ultracut UCT; Leica Microsystems, Buffalo Grove, IL) to obtain slices with ~70 nm thickness. Subsequently, specimens were placed on carbon-coated copper grids and stained with alcoholic uranyl acetate.[31] Samples were finally stained with saturated methanolic uranyl acetate (5 minutes) and Venable and Coggeshall's lead citrate (5 minutes).[24] All experiments in this research followed the protocols approved by the Animal Care Committee (ACC) at the University of Illinois at Chicago, and conformed to the statement on the Use of Animals in Ophthalmic and Vision Research, established by the Association for Research in Vision and Ophthalmology (ARVO).

Experimental Setup

A NIR light microscope (BX531 WI; Olympus, Center Valley, PA) with a 60X water immersion objective (UMPLFLN60XW; Olympus, Center Valley, PA) and a CCD camera (Neo 5.5; Andor Technology, Concord, MA) were used to record the light-evoked responses of isolated rod OSs. The visible stimulus was provided by a fiber-coupled light emitting diode (LED; central wavelength: 550 nm, bandwidth: ~200 nm) and was then coupled into the microscope to illuminate the whole sample. The stimulus intensity was empirically set to ~1.13×10^8 photon·$\mu m^{-2} \cdot s^{-1}$ to enable a robust shrinkage of rod OS. The image acquisition rate was set to 100 frames per second and each imaging trial lasted 3 seconds, including a 1-second prestimulus phase, a 1-second stimulus phase, and a 1-second poststimulus phase. The CCD camera and LED were hardware-synchronized and software-controlled by a custom-designed LabView (National Instrument, Austin, TX) program.

The histological images of retina slices were acquired using a light microscope (Axiovert 100M; Zeiss, Thornwood, NY) and a 20× objective (Plan-Neofluar; Zeiss, Thornwood, NY). TEM imaging was achieved using a TEM (JEM-1220; JEOL, Peabody, MA) at 120 kV fitted with a LaB6 electron source and a CCD camera (Es1000W 11MP; Gatan, Weinheim, Germany).

Image Processing and Data Analysis

In the time-lapse light microscopic study, the time course of the shrinkage magnitude of rod OS length and diameter was used to reveal the stimulus-evoked morphological changes of rod OSs (Fig. 1C). For each recording trial, the length and diameter of the isolated rod OS in each image were measured. Therefore, 300 pairs of the lengths and diameters of the rod OS under monitoring were obtained throughout the experiment with a temporal resolution of 10 ms. The magnitude of rod OS length or diameter shrinkage at a certain time point was considered as the difference between the rod OS length or diameter in the corresponding image and that of the first image.

Both OS and inner segment (IS) lengths were obtained from rod photoreceptors with an intact structure in the histological images of retinas. As the histological images of retinas presented clear struc-
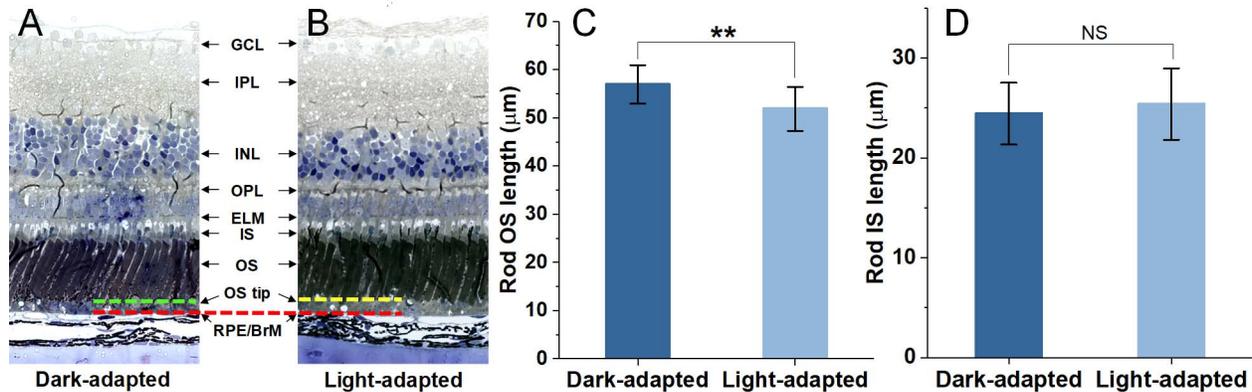
Figure 2. Histological images of eyecups from the dark-adapted eye (A), and the light-adapted eye (B). The *green dashed line* in A and the *yellow-dashed line* in B represent the general position of OS tips in dark- and light-adapted samples, respectively. The *red-dashed line* indicates BrM. Statistics of rod OS length (C) and IS length (D) in dark- and light-adapted samples. For each group of data, a total of ~130 measurements were obtained from seven retinas. Data are the mean and standard deviation. Significance was determined with two-tailed Student's t-test with **$P < 0.05$; NS, not significant. GCL, ganglion cell layer; IPL, inner plexiform layer; INL, inner nuclear layer; RPE, retinal pigment epithelium.

tures of retinal cells and different retinal layers (Figs. 2A, 2B), the rod OS length was defined as the axial distance between the OS tip and OS/IS intersection, and the rod IS length was the distance between the external limiting membrane (ELM) and the OS/IS intersection. The images were acquired from similar retinal locations (~1.8 mm) relative to the optical nerve head in each eye to avoid intrinsic differences of retinal structures due to different retinal regions. Approximately 20 rod photoreceptors from each eye were selected for measurement. A total number of 260 measurements from 14 eyes (seven dark-adapted and seven light-adapted) were further processed for statistical analysis.

In TEM study, rod OSs with relatively uniform structure (as indicated by black-dashed rectangles in Figs. 3A1–3A3) were first selected from TEM images with low magnification (4 kX). These rod OSs then underwent imaging with high magnification (150 kX) and local regions with parallel discs (Fig. 3B) presented were further selected for inter- and intradisc distance measurement. As shown in Figure 3D, the interdisc distance is defined as the distance between the disc membranes of two adjacent discs, and the intradisc distance is defined as the thickness, including the lipid bilayers, of the disc. The TEM images used for measurements were acquired at magnifications of 150 kX with a pixel resolution of 0.36 nm/pixel. Each TEM image was divided into 400 subwindows and 10 of them were randomly selected for measurement to minimize the personal preference of the observer. Given the nanometer level resolution of TEM, edges of the discs could be clearly identified, which further

enabled solid quantification of geometric variations of the discs. One interdisc distance and one intradisc distance was then obtained from each of the 10 subwindows. The inter- and intradisc distances were further categorized into three groups, that is, tip, middle, and base, according to the corresponding disc location in the rod OS (Fig. 3A1). As a result, a total of ~1000 measurements of interdisc distance were obtained and the same amount of measurements of intradisc distances were evenly collected from the tip, middle, and base regions of 62 individual rods of five dark-adapted and five light-adapted retinal samples (e.g., ~160 measurements of intradisc distances from the tip region of dark-adapted rod OS). Kolmogorov-Smirnov tests were performed to validate the normality of the measurements. Data sets were expressed as the mean and standard deviation.

Based on the measurements obtained from histological and TEM images of rod OSs, the shrinkage ratio was defined to investigate the relationship between the overall rod OS shrinkage and the structural perturbation of disc stacks, respectively. In the histological study, the light-induced shrinkage ratio was defined as:

$$\left(\overline{OSL}_D - \overline{OSL}_L\right)\Big/\overline{OSL}_D \qquad (1)$$

where $\overline{OSL}_D$ is the averaged rod OS length in dark-adapted samples and $\overline{OSL}_L$ is the averaged rod OS length in light-adapted samples. In the TEM study, the light-induced shrinkage ratio in a disc stack containing N discs was defined as:
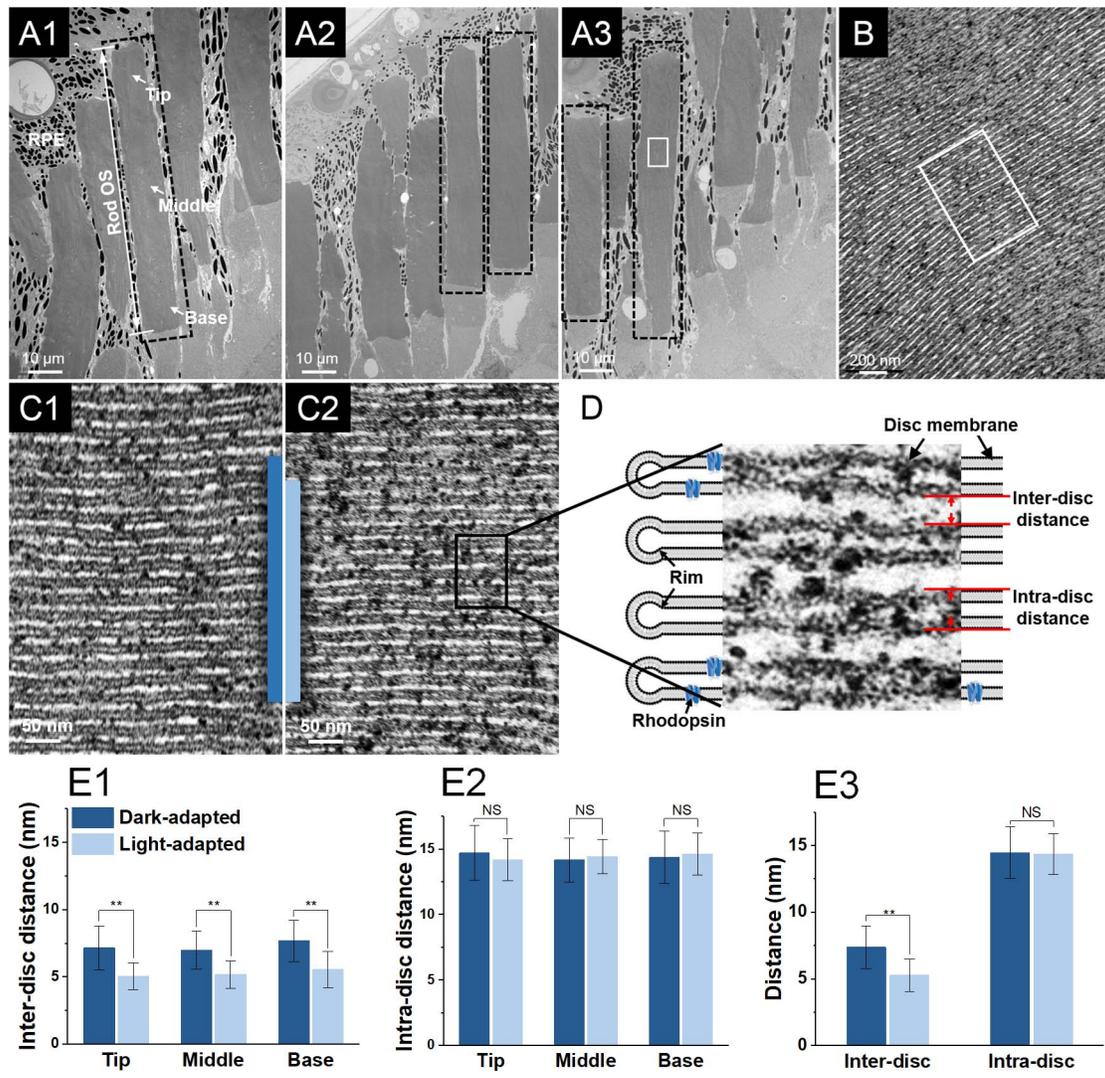
Figure 3. (A1–A3) Representative TEM images of a frog retina, including photoreceptors, RPE cells, and melanosomes (*black particles*), at low magnification (4 kX). The tip, middle, and base regions of the rod OSs are as indicated in A1. The *black-dashed rectangles* demonstrate the rod OSs with relatively uniform structure. (B) TEM image of the lamellar structure of discs in the *white rectangle* in A3 obtained with a magnification of 150 kX. (C1) Enlarged image of the discs in the *white rectangle* in B (dark-adapted sample). (C2) Corresponding TEM image of the discs from a light-adapted sample, obtained with same TEM magnification. (D) Cartoon and TEM image illustration of the rod OS discs and the corresponding inter- and intradisc distances. Statistics of interdisc distances (E1) and intradisc distances (E2) in the tip, middle, and base regions of rod OSs in dark- and light-adapted samples. $n = 5$ for each bar. (E3) Statistics of inter- and intradisc distances in dark- and light-adapted samples. $n = 5$ for each bar. Data are the mean and standard deviation. Significance was determined with a two-tailed Student's t-test with **$P < 0.05$; NS, not significant.

$$[N \cdot (d_{interD} + d_{intraD}) - N \cdot (d_{interL} + d_{intraL})]/$$
$$[N \cdot (d_{interD} + d_{intraD})] \quad (2)$$

where d_{interD} and d_{interL} are the interdisc distance in dark- and light-adapted samples, respectively, and d_{intraD} and d_{intraL} are the intradisc distances in dark- and light-adapted samples, respectively.

Results

Time-Lapse Light Microscopy of Rod OS Shrinkage

In this study, time-lapse light microscopy was employed to provide direct observation of the rod OS length shrinkage evoked by a visible light stimulus. Figure 1A shows time-lapse light microscopic images

of a representative single isolated rod OS obtained before, during, and after a 1-second stimulus. The onset time of the stimulus was set as time 0 second. Figure 1B provides an enlarged illustration of the images of the rod OS tips indicated by the white rectangle in Figure 1A. As shown in Figure 1B, the increased distance between the tip of the rod OS and the black-dashed line demonstrates a significant length shrinkage of the rod OS after the onset of the stimulus (also see the Supplementary Movie 1 and 2). The averaged magnitude of rod OS length and diameter shrinkage over time (from eight isolated rod OSs from four retinas) are shown in Figure 1C. The waveform of the length shrinkage shows a stable and flat stage before the stimulus presentation and a rapid rise upon the stimulus initiation, indicating the length shrinkage is directly correlated with the stimulus. However, the flat waveform of the diameter shrinkage showed that the rod OS diameter was not affected by the stimulation and maintained a consistent scale during the experiment. The relationship of the standard deviation amplitudes to the mean waveform reflects a general similarity of the stimulus-evoked responses observed from different rod OSs.

Comparative Histological Study of the Retina in Dark- and Light-Adapted Eyes

To verify the light-induced length shrinkage of rod OSs in the intact retina, histological examinations were conducted on dark- and light-adapted frog eyes. Figures 2A and 2B show representative transmission microscopic images of eyecup slices from dark- and light-adapted eyes, respectively. As shown in the images, two retinas exhibited a similar overall thickness and comparable locations of the ELM and outer plexiform layer (OPL). As Bruch's membrane (BrM) layers in the two images were horizontally aligned (marked by the red-dashed line), the light-adapted retina presented significantly increased distances between the rod OS tips (marked by the yellow-dashed line) and BrM, compared to that of the dark-adapted retina (the distance between green- and red-dashed lines). To validate the reliability and repeatability of the observations, the lengths of rod OSs were measured from a total of 260 retinal locations in seven pairs of dark- and light-adapted frog eyes. The corresponding rod IS length was also measured from the same retinal locations as a reference. The statistical results shown in Figures 2C and 2D revealed that rod OS lengths were significantly reduced in light-adapted eyes (51.8 ± 4.5 μm)

compared to those of dark-adapted eyes (56.9 ± 3.9 μm). However, the differences between rod IS lengths were not significant (24.4 ± 3.1 μm and 25.4 ± 3.6 μm in dark- and light-adapted eyes, respectively).

Comparative TEM Study of Rod Discs in Dark- and Light-Adapted Eyes

As previous time-lapse light microscopic and histological studies have confirmed the light-induced length decreases in rod OSs, the following aim of this study was to disclose the anatomic source of the rod OS shrinkage on a subcellular level. Our previous studies suggested the conformational change of rod OSs was correlated with the phototransduction cascades on or adjacent to the discs. Therefore, we hypothesized the overall rod OS shrinkage was related to the perturbation of the lamellar structure of the rod discs. To verify the hypothesis, comparative TEM studies were conducted on rod OSs under light- and dark-adapted conditions. Figures 3A1 to 3A3 show representative overall views of the photoreceptors under TEM in which individual rods can be clearly identified. Figure 3B shows the well-preserved lamellar structure of the discs in the white rectangle in Figure 3A3, obtained with high TEM magnification. Figures 3C1 and 3C2 are representative TEM images of disc stacks in the dark- and light-adapted rod OSs, respectively. To provide a direct impression of how light illumination changed the lamellar structure of the discs, two blue bars, with each bar covering 15 discs, were placed in the images with their bottoms horizontally aligned. The blue bar in the light-adapted rod OS is significantly shorter in length, compared with that in the dark-adapted rod OS, indicating the light adaptation reduced the length of the disc stacks. As shown in Figure 3D, to demonstrate whether the reduction in length came from the distance between the discs (interdisc distance), the disc itself (intradisc distance) or from both, the inter- and intradisc distances were measured in both dark- and light-adapted samples and statistically compared to illustrate the difference. Further, the inter- and intradisc distances were compared based on their relative locations, that is, tip, middle, or base region (Fig. 3A1), in the rod OSs. The means and standard deviations of the measurements are summarized in the Table. As shown in Figures 3E1 to 3E3, the statistical analysis demonstrated that the light illumination resulted in a significant decrease in the interdisc distances from all three regions and the overall

Table. Means and Standard Deviations of the Inter- and Intradisc Distances Measured From Tip, Middle, and Base Regions of Dark- and Light-Adapted Rod Photoreceptors (the Unit is Nanometers)

	Tip	Middle	Base	Avg.
Dark-adapted				
Interdisc	7.15 ± 1.64	6.98 ± 1.40	7.69 ± 1.55	7.38 ± 1.61
Intradisc	14.71 ± 2.07	14.17 ± 1.67	14.36 ± 1.98	14.46 ± 1.92
Light-adapted				
Interdisc	5.04 ± 0.99	5.17 ± 1.02	5.55 ± 1.34	5.28 ± 1.21
Intradisc	14.18 ± 1.60	14.43 ± 1.32	14.62 ± 1.60	14.36 ± 1.51

interdisc distance, but barely affected the intradisc distances.

Discussion

In this study, we employed multiple imaging modalities to explore the anatomic source of light-correlated rod OS shrinkage. Using time-lapse light microscopy, we directly observed robust length shrinkage in single isolated rod OSs when a visible light stimulus was applied (Fig. 1). As the rod IS was absent in this experiment, we verified that the rod OS itself can trigger the shrinkage. However, as the behavior of rod photoreceptors could be vulnerable in an in vitro environment, the light-induced structural changes were further investigated in the intact retina by comparing the histological sections of retinas from dark- and light-adapted eyes. Benefiting from the high spatial resolution of light microscopic images, the structure of the retina can be clearly identified, enabling precise measurement of rod OS and IS lengths. The statistical analysis proved that light illumination introduced a significant length decrease in rod OSs but did not affect the length of rod ISs. Moreover, the rapid time course, that is, almost immediate onset time of the shrinkage, and the rapid time-to-peak of the shrinkage shown in Figure 1C do not favorably support the possible causes related to the relatively slow physiological processes, such as translocation of signaling proteins[32] and apical process of RPE cells.[25,33] Combining these observations, our results suggested that the mechanical origin of OS length shrinkage was within the OS.

To further explore the structural changes within the rod OSs, TEM was employed to provide images of disc stacks with resolution at the nanometer level. TEM images obtained in this study exhibited the lamellar structure of the rod discs and provided clear identification of the disc membranes and the spaces within the discs (white areas between disc membranes) (Figs. 3B, C1, 3C2).[34] Two dimensions, the inter- and intradisc distance, that is, the thickness of the disc and distance between the discs, were then quantified to illustrate the perturbation. To reflect the general configuration of the discs, OS regions with the structure of paralleled discs were selected to measure the inter- and intradisc distances for our statistical analysis. Sampling from these regions principally guaranteed the continuity and reliability of the measurements by avoiding structural distortions caused by artifacts from the sample preparation. We also noted that the fixation processing during the retinal preparation could potentially introduce dimensional changes to the samples, but its influence on the reliability of the result was minimized as all our dark- and light-adapted samples underwent exactly the same fixation procedures. The structure of rod OS discs presented, and the inter- and intradisc distance measured in this study were also consistent with previous publications.[27,28,35,36] As a result, the interdisc distance was found to present a significant shrinkage rather than the intradisc distance. In addition, the inter- and intradisc distances at different locations, that is, tip, middle, and base regions, of the rod OSs were compared. The results showed that a significant decrease was consistently observed in the interdisc distances of all three regions, indicating the shrinkage was a general phenomenon along the axial direction of the rod OSs. Therefore, the rod OS shrinkage observed in this study was caused by the reduction of interdisc space, not changes in the discs themselves that were related with osmotic volume change[37] or lateral expansion of the disc membranes proposed in previous studies.[38]

The shrinkage ratio of rod OSs obtained in the histological study was similar to that of the disc stacks in the TEM study. As defined by equations (1) and (2), the shrinkage ratio of rod OSs in the histological

study was ~0.089 and the shrinkage ratio of disc stacks in the TEM study was ~0.101 (calculated by the means of corresponding data). As the disc stacks (include both inter- and intradisc space) occupy most of the photoreceptor OS, such similarity further suggests that the overall rod OS length shrinkage was correlated with the reduction of the space between discs. Because the rhodopsin, transducin and PDE are anchored to the lipid bilayer of the disc, the shrinkage in the interdisc space then must have a more direct correlation with the cascaded reactions happening between the discs.

Furthermore, different from the shrinkage in rod OS length, we did not observe any reliable changes in the diameters of the isolated rod OSs before, during, or after the light stimulus, indicating the total volume of the rod OS was reduced during the shrinkage (Fig. 1C). However, the reduction in rod OS volume was unlikely related to the intracellular osmotic change caused by the light-induced closure of cGMP-gated ion channels. Evidence can be found in our previous observation of persistent light-induced rod OS movement, which was associated with unbalanced OS shrinkage, in a low-sodium medium.[19] Therefore, the interdisc space shrinkage is probably not a consequence of the blockage of rod circulating current and must have a more complicated mechanism.[35,39,40]

In summary, this study confirmed the light-induced rod OS shrinkage with multiple imaging modalities and demonstrated its anatomical origin was correlated with a reduction of the interdisc space, instead of the thickness of the disc itself, in the rod OS. Better understanding of the principle behind the OS shrinkage will not only benefit our knowledge of the phototransduction, but also may provide insights for instrument design to achieve functional imaging of photoreceptor physiology.

Acknowledgments

Disclosure: **Y. Lu**, None; **J. Benedetti**, None; **X. Yao**, None

References

1. Arshavsky VY, Lamb TD, Pugh EN. Jr G proteins and phototransduction. *Ann Rev Physiol*. 2002;64:153–187.
2. Brown JE, Pinto LH. Ionic mechanism for the photoreceptor potential of the retina of Bufo marinus. *J Physiol*. 1974;236:575–591.
3. Lamb TD, Pugh EN Jr. Phototransduction, dark adaptation, and rhodopsin regeneration the proctor lecture. *Invest Ophthalmol Vis Sci*. 2006; 47:5137–5152.
4. Hofmann KP, Schleicher A, Emeis D, Reichert J. Light-induced axial and radial shrinkage effects and changes of the refractive index in isolated bovine rod outer segments and disc vesicles: physical analysis of near-infrared scattering changes. *Biophys Struct Mech*. 1981;8:67–93.
5. Hofmann KP, Uhl R, Hoffmann W, Kreutz W. Measurements on fast light-induced light-scattering and -absorption changes in outer segments of vertebrate light sensitive rod cells. *Biophys Struct Mech*. 1976;2:61–77.
6. Pepperberg DR, Kahlert M, Krause A, Hofmann KP. Photic modulation of a highly sensitive, near-infrared light-scattering signal recorded from intact retinal photoreceptors. *Proc Natl Acad Sci U S A*. 1988;85:5531–5535.
7. Vuong TM, Pfister C, Worcester DL, Chabre M. The transducin cascade is involved in the light-induced structural changes observed by neutron diffraction on retinal rod outer segments. *Biophys J*. 1987;52:587–594.
8. Yao X, Wang B. Intrinsic optical signal imaging of retinal physiology: a review. *J Biomed Opt*. 2015;20:090901.
9. Cooper RF, Tuten WS, Dubra A, Brainard DH, Morgan JI. Non-invasive assessment of human cone photoreceptor function. *Biomed Opt Exp*. 2017;8:5098–5112.
10. Curcio CA, Medeiros NE, Millican CL. Photoreceptor loss in age-related macular degeneration. *Invest Ophthalmol Vis Sci*. 1996;37:1236–1249.
11. Jackson GR, Owsley C, Curcio CA. Photoreceptor degeneration and dysfunction in aging and age-related maculopathy. *Ageing Res Rev*. 2002;1: 381–396.

12. Portera-Cailliau C, Sung C, Nathans J, Adler R. Apoptotic photoreceptor cell death in mouse models of retinitis pigmentosa. *Proc Natl Acad Sci*. 1994;91:974–978.

13. Zhao X, Thapa D, Wang B, Lu Y, Gai S, Yao X. Stimulus-evoked outer segment changes in rod photoreceptors. *J Biomed Opt*. 2016;21:065006–065006.

14. Lu Y, Liu C, Yao X. In vivo super-resolution imaging of transient retinal phototropism evoked by oblique light stimulation. *J Biomed Opt*. 2018;23:050502.

15. Abramoff MD, Mullins RF, Lee K, et al. Human photoreceptor outer segments shorten during light adaptation. *Invest Ophthalmol Vis Sci*. 2013;54:3721–3728.

16. Lu R, Levy AM, Zhang Q, Pittler SJ, Yao X. Dynamic near-infrared imaging reveals transient phototropic change in retinal rod photoreceptors. *J Biomed Opt*. 2013;18:106013.

17. Zhang QX, Zhang Y, Lu RW, et al. Comparative intrinsic optical signal imaging of wild-type and mutant mouse retinas. *Opt Express*. 2012;20:7646–7654.

18. Zhang Q-X, Lu R-W, Curcio CA, Yao X-C. In vivo confocal intrinsic optical signal identification of localized retinal dysfunction functional imaging of retinal photoreceptors. *Invest Ophthalmol Vis Sci*. 2012;53:8139–8145.

19. Lu Y, Wang B, Pepperberg DR, Yao X. Stimulus-evoked outer segment changes occur before the hyperpolarization of retinal photoreceptors. *Biomed Opt Exp*. 2017;8:38–47.

20. Nilsson SEG. An electron microscopic classification of the retinal receptors of the leopard frog (Rana pipiens). *J Ultrastruct Res*. 1964;10:390–416.

21. Carter-Dawson LD, Lavail MM. Rods and cones in the mouse retina. I. Structural analysis using light and electron microscopy. *J Comparative Neurol*. 1979;188:245–262.

22. Boyer NP, Chen C, Koutalos Y. Preparation of living isolated vertebrate photoreceptor cells for fluorescence imaging. *J Vis Exp*. 2011;52:2789.

23. Chen C, Jiang Y, Koutalos Y. Dynamic behavior of rod photoreceptor disks. *Biophys J*. 2002;83:1403–1412.

24. Tam BM, Yang LL, Bogėa TH, Ross B, Martens G, Moritz OL. Preparation of Xenopus laevis retinal cryosections for electron microscopy. *Exp Eye Res*. 2015;136:86–90.

25. Zhang Q-X, Lu R-W, Messinger JD, Curcio CA, Guarcello V, Yao X-C. In vivo optical coherence tomography of light-driven melanosome translocation in retinal pigment epithelium. *Sci Rep*. 2013;3.

26. Usukura J, Yamada E. Molecular organization of the rod outer segment. A deep-etching study with rapid freezing using unfixed frog retina. *Biomed Res*. 1981;2:177–193.

27. Nilsson SEG. The ultrastructure of the receptor outer segments in the retina of the leopard frog (Rana pipiens). *J Ultrastruct Res*. 1965;12:207–231.

28. Bachhuber K, Frösch D. Electron microscopy of melamine-embedded frog retina: evidence for the overall crystalline organization of photoreceptor outer segments. *J Microscopy*. 1984;133:103–109.

29. Fliesler SJ, Rayborn ME, Hollyfield JG. Membrane morphogenesis in retinal rod outer segments: inhibition by tunicamycin. *J Cell Biology*. 1985;100:574–587.

30. Brubacher JL, Vieira AP, Newmark PA. Preparation of the planarian Schmidtea mediterranea for high-resolution histology and transmission electron microscopy. *Nature Protocols*. 2014;9:661.

31. Jones G. Electron microscopy of frog photoreceptor outer segments after fixation with aldehydes. *J Cell Sci*. 1974;16:199–219.

32. Calvert PD, Strissel KJ, Schiesser WE, Pugh EN, Arshavsky VY. Light-driven translocation of signaling proteins in vertebrate photoreceptors. *Trends Cell Biol*. 2006;16:560–568.

33. Strauss O. The retinal pigment epithelium in visual function. *Physiol Rev*. 2005;85:845–881.

34. Steinberg RH, Fisher SK, Anderson DH. Disc morphogenesis in vertebrate photoreceptors. *J Comparative Neurol*. 1980;190:501–518.

35. Korenbrot JI, Brown DT, Cone RA. Membrane characteristics and osmotic behavior of isolated rod outer segments. *J Cell Biol*. 1973;56:389–398.

36. Nir I, Pease DC. Ultrastructural aspects of discs in rod outer segments. *Exp Eye Res*. 1973;16:173–182.

37. Heller J, Ostwald TJ, Bok D. The osmotic behavior of rod photoreceptor outer segment discs. *J Cell Biol*. 1971;48:633–649.

38. Asai H, Chiba T, Kimura S, Takagi M. A light-induced conformational change in rod photoreceptor disc membrane. *Exp Eye Res*. 1975;21:259–267.

39. Hagins W, Penn R, Yoshikami S. Dark current and photocurrent in retinal rods. *Biophysical J*. 1970;10:380–412.

40. Yagi N. Structural changes in rod outer segments of frog and mouse after illumination. *Exp Eye Res*. 2013;116:395–401.